Thermodynamics, Structure, and Dynamics in Room Temperature Ionic Liquids: The Case of 1-Butyl-3-methyl Imidazolium Hexafluorophosphate ([bmim][PF_6])

Alessandro Triolo,*,†,|| Andrea Mandanici,‡,|| Olga Russina,§ Virginia Rodriguez-Mora,|| Maria Cutroni,‡ Christopher Hardacre,⊥ Mark Nieuwenhuyzen,⊥ Hans-Jurgen Bleif,§ Lukas Keller,# and Miguel Angel Ramos*,||

Istituto per i Processi Chimico-Fisici, Consiglio Nazionale delle Ricerche, via La Farina 237, 98123 Messina, Italy, Dipartimento di Fisica, Università di Messina, 98100 Messina, Italy, Hahn-Meitner Institut, Glienicker Street 100, D-14109 Berlin, Germany, Laboratorio de Bajas Temperaturas, Departamento de Fisica de la Materia Condensada, C-III, Universidad Autonoma de Madrid, Cantoblanco, E-28049 Madrid, Spain, QUILL Research Centre and School of Chemistry and Chemical Engineering, Queen's University, Belfast, BT9 5AG, Northern Ireland, and Laboratory for Neutron Scattering, ETH Zurich and Paul Scherrer Institute, 5232 Villigen PSI, Switzerland

Received: May 11, 2006; In Final Form: July 6, 2006

A detailed investigation of the phase diagram of 1-butyl-3-methyl imidazolium hexafluorophosphate ([bmim][PF_6]) is presented on the basis of a wide set of experimental data accessing thermodynamic, structural, and dynamical properties of this important room temperature ionic liquid (RTIL). The combination of quasi adiabatic, continuous calorimetry, wide angle neutron and X-ray diffraction, and quasi elastic neutron scattering allows the exploration of many novel features of this material. Thermodynamic and microscopic structural information is derived on both glassy and crystalline states and compared with results that recently appeared in the literature allowing direct information to be obtained on the existence of two crystalline phases that were not previously characterized and confirming the view that RTILs show a substantial degree of order (even in their amorphous states), which resembles the crystalline order. We highlight a strong connection between structure and dynamics, showing the existence of three temperature ranges in the glassy state across which both the spatial correlation and the dynamics change. The complex crystalline polymorphism in [bmim][PF_6] also is investigated; we compare our findings with the corresponding findings for similar RTILs. These results provide a strong experimental basis for the exploration of the features of the phase diagram of RTILs and for the further study of longer alkyl chain salts.

Introduction

Room temperature ionic liquids (RTILs) is the term that is presently used to identify a neoteric class of organic salts that show a melting point below ambient temperature. These are typically built up by a bulky, asymmetric organic cation, such as 1-alkyl-3-methyl imidazolium, and a fluorine-containing anion, such as $[PF_6]^-$. RTILs are attracting great attention for their low melting point and limited vapor pressure, which make them ideal solvents for green chemistry.[1,2] RTILs are often denoted as designer solvents because of the versatility of their properties, which is a consequence of the ease of interexchanging anions and cations that lead to a huge number of combinations. They are characterized by a wide spectrum of bulk properties, such as viscosity, conductivity, solvating properties, etc.

In this study, we report on quasi-adiabatic, continuous calorimetry measurements on a prototype RTIL, 1-butyl-3-methyl imidazolium hexafluorophosphate ([bmim][PF_6]). The corresponding thermodynamic information has been complemented with both structural and dynamic information derived from X-ray and neutron diffraction, providing a detailed insight into the many issues on the phase diagram of this system. Similarly to what has been found in other $[bmim]^+$-based RTILs, we characterize for the first time in [bmim][PF_6] the thermodynamic and structural features of polymorphism in the crystalline state, highlighting the existence of two different crystalline phases for [bmim][PF_6]. This morphological feature of $[bmim]^+$-based RTILs has been proposed as a plausible rationalization of their low melting point and their good glass-forming ability. The complementary use of calorimetry, diffraction, and quasi elastic scattering techniques (QENS) provides a wide spectrum of information on all the different phases of [bmim][PF_6].

The tendency to crystallize at a low enough temperature might be a potential limitation for some RTILs, especially when one wishes to use them at temperatures below ambient conditions. For this reason, a detailed understanding of the phase diagram of RTILs is of high importance to further extend the range of applications for these important green materials. Because of the growing importance of RTILs, many properties of [bmim][PF_6] were recently investigated. Information on synthesis and applications of [bmim][PF_6] were provided a decade ago.[3] Information on its phase diagram (melting point, stability temperature range, density, viscosity, etc.) also were reported.[4]

* Corresponding authors. E-mail addresses: (A. Triolo) triolo@me.cnr.it; (M. A. Ramos) miguel.ramos@uam.es.
† Istituto per i Processi Chimico-Fisici, Consiglio Nazionale delle Ricerche.
‡ Università di Messina.
§ Hahn-Meitner Institut.
|| Universidad Autonoma de Madrid.
⊥ Queen's University.
ETH Zurich and Paul Scherrer Institute.

10.1021/jp062895t CCC: $33.50
Published on Web 09/22/2006

More recently, thermodynamic properties both in the ideal gas state[5] and in the condensed state[6] were reported. The latter accurate and extensive study contains valuable information, which complements our present calorimetric study in which the main goal is to provide a thermal characterization of the [bmim][PF_6] phase diagram.

Experimental Section

Sample. 1-Butyl-3-methyl imidazolium hexafluorophosphate, [bmim][PF_6], was purchased from Solvent Innovation. The residual chloride content was <7 ppm, as determined by ion chromatography,[7] and the water content, which was determined by Karl Fischer titration, was found to be 0.0364 wt % before drying and 0.0124 wt % after drying. Little hydrolysis of the anion was observed using ion chromatography with a fluoride concentration of <5 ppm. Analysis of the sample by ^{1}H NMR indicated that any impurities, for example, residual *N*-methylimidazole, were below the detection limit. Before all the measurements, the sample was kept under vacuum at 40 °C for at least 24 h, which allowed moisture and volatile components to be eliminated. Fully deuterated [bmim][PF_6] was prepared from deuterated 1-butyl-3-methyl imidazolium chloride salts[8] by metathesis with ND_4PF_6 in D_2O using the standard procedure.[9] The sample was analyzed by ^{1}H and ^{2}H NMR, as well as by elemental analysis, and showed >97% deuterium incorporation.

Calorimetry. Calorimetric measurements were performed using a cylindrical cell of aluminum (13 mm in diameter, 25 mm in height) with very thin walls (0.3 mm) and with an aluminum cap that was indium sealed. Possible mass leaks were previously discarded after exposing the cell to a dynamic vacuum from a diffusive pump. A second check on the total mass of the measurement cell full of liquid was performed at the end of each measurement run. The cell was suspended from the inner flange of the cryostat by nylon threads. An electric heater ($\approx$1 kΩ) and a standard silicon diode operating at 10 μA were attached to the thin walls of the sample holder. The total weight of the empty cell was 5.43 g, and the amount of [bmim][PF_6] put inside the cell was 4.147 g. The heat capacity of the empty cell was measured independently and under the same conditions to subtract its contribution. Experiments were run in a glass cryostat by using nitrogen as cryogenic liquid and were conducted in a high-vacuum environment ($\leq 10^{-7}$ mbar).

Because the measurements were made in a sealed calorimeter under their own vapor pressure, the obtained data were heat capacities at saturation pressure C_s. However, their differences with the usual heat capacities at constant pressure C_p were negligible, especially given the very low vapor pressure of [bmim][PF_6], and the latter term will be used hereafter. Specific-heat data presented in this work were obtained by employing a quasi-adiabatic, continuous method.[10] The calorimetric cell was in contact with the thermal reservoir at 77 K through an effective thermal link (mainly arising from blackbody thermal radiation plus conduction through the electrical wiring). Therefore, the equation of heat transport contains both cooling P_{cool} and heating P_{heat} power terms, so that

$$C_p\left(\frac{dT}{dt}\right) = P_{heat} + P_{cool} = V_h I_h + C_p \dot{\tau}(T) \qquad (1)$$

where V_h and I_h are the voltage applied to the heater element and the electric current flowing through it, respectively, and $\dot{\tau}(T)$ is the intrinsic (negative) thermal drift of the system, which is directly measured as a function of temperature by standard cooling at $I_h = 0$ with the thermal reservoir fixed at 77 K. Therefore, the heat capacity of the cell can be determined from

$$C_p = \frac{V_h I_h}{\left(\frac{dT}{dt} - \dot{\tau}(T)\right)} \qquad (2)$$

Alternatively, a direct display of the measured dT/dt curve as a function of temperature T for a constant applied power is a useful method to investigate first-order transitions such as melting and crystallization processes.

Comparisons from different methods and with other literature data in several other studied substances lead us to estimate an accuracy for the absolute heat-capacity data of better than 4% between 77 and 200 K.[11]

QENS.[12] Elastic fixed energy scans (EFES) were collected at both IN16 and IN10 at the Institute Laue-Langevin (ILL) using $\lambda = 6.271$ Å and accessing a Q range between 0.43 and 1.90 Å^{-1} with an energy resolution of 0.9 μeV. The EFES data were collected as a function of temperature by monitoring the number of neutrons that were elastically scattered by heating or cooling the sample, following removal of the constant contribution from the empty cell and the normalization of the detector efficiency using vanadium. The measurements were collected from samples that were contained in cylindrical annular aluminum cells with the sample thickness being between 0.1 and 0.5 mm to minimize multiple scattering effects. To access the dynamical features related to the amorphous glass, cooling from the melt was chosen to avoid crystallization of the sample, which occurs upon heating the glassy amorphous phase. The samples were investigated between ca. 10 to 450 K using heating/cooling rates of 1.3 K min^{-1}. EFES were also collected at IN10 (that is a backscattering spectrometer similar to IN16) at the same experimental conditions.

Inelastic fixed energy scans (IFES) were collected at the BSS spectrometer at the Forschungszentrum Juelich (FZJ) by using an energy resolution of approximately 1 μeV, which covered a Q range between 1.02 and 1.87 Å^{-1}. During the measurements, the number of neutrons that were scattered from the sample with an energy exchange of 14.15 μeV was monitored upon heating/cooling, covering a temperature range between 10 and 450 K. The same cylindrical annular sample geometry that was used at the ILL was used for these experiments.

Neutron Diffraction. Wide angle neutron scattering (WANS) measurements were collected on fully deuterated [bmim][PF_6] at the DMC diffractometer[13] (using the wavelength $\lambda = 2.569$ Å) at the Paul Scherrer Institut (PSI). The sample was contained in a cylindrical cell with a diameter of 0.7 cm. The glassy sample was obtained by fast cooling of the sample inside the available cryostat, and the absence of Bragg peaks associated with crystalline phases indicated that the glassy state was obtained.

X-ray Diffraction. Wide angle X-ray diffraction data were collected on [bmim][PF_6] using a low-temperature Guinier diffractometer manufactured by Huber (type 645) that operated at the wavelength $\lambda = 1.54$ Å. The sample was sandwiched between two amorphous plastic foils, and the contribution of these foils subsequently was subtracted. The instrument allowed the collection of data from 100 K up to room temperature, which covered a Q range between 0.7 and 5.0 Å^{-1}.

Results and Discussion

I. Glassy State. Glassy [bmim][PF_6] can be obtained easily by cooling below the glass transition from the liquid state at room temperature. We observed that our samples crystallized

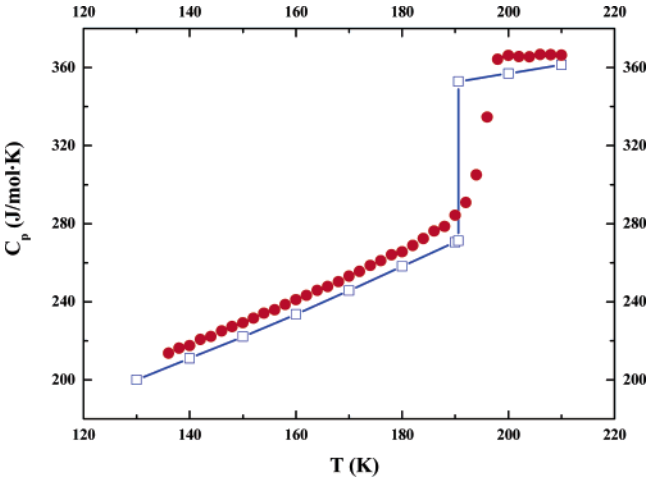

Figure 1. Molar specific heat of glassy [bmim][PF_6] in the temperature range between 140 and 210 K. The blue open squares are data from Kabo et al.[6]

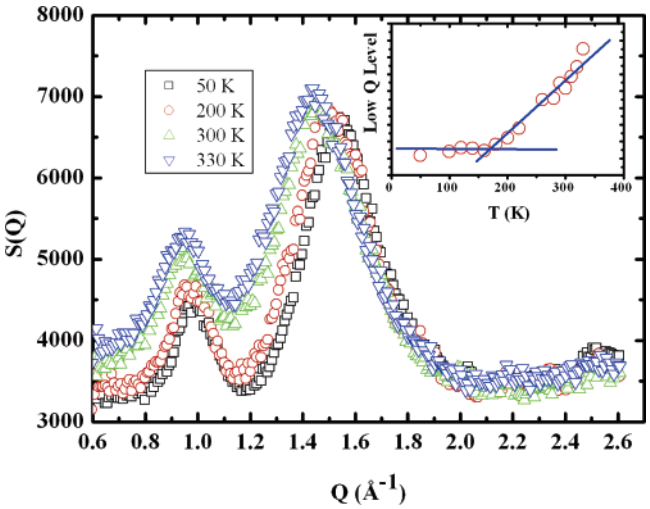

Figure 2. WANS data for the amorphous glass and the fully deuterated liquid [bmim][PF_6] at selected temperatures (50, 200, 300, and 330 K). In the inset, the temperature dependence of the limit intensity value at low Q (average over the interval: $0.6 < Q$ (Å^{-1}) < 0.7) is plotted.

when cooled at slow rates ($\leq$0.02 K s^{-1}), while faster cooling rates successfully led to the amorphous solid or glass below T_g. In agreement with ref 6, upon heating the amorphous glass, the crystallization of the supercooled liquid started at around T = 220 K. The molar specific heat (M_w = 284.18 g mol^{-1}) of glassy [bmim][PF_6] in the temperature range between 120 and 205 K, which was determined as explained in the previous section, is presented in Figure 1. Our heat-capacity measurements were in reasonable agreement with the data reported in ref 6. We obtained a glass-transition temperature (T_g = 194 K), which was 3 K higher than that reported in ref 6. The discontinuity in the specific heat was in good agreement with the reported value of $\Delta C_p(T_g)$ = 81.6 J/(K·mol) (ref 6). We also observed the melting temperature of crystalline [bmim][PF_6] to occur at T_m = 284 K, which again was in good agreement with Kabo et al.[6] Hence, the ratio T_g/T_m = 0.68 was obtained, which is typical for a good glass formation.

The thermodynamic magnitudes involved in the (crystal−liquid) melting transition and in the (amorphous solid−liquid) glass transition often have been rationalized in terms of "beads", that is, more or less compact, movable units that conform to the molecule and to their corresponding degrees of freedom. Concerning the glass transition, we obtained $\Delta C_p(T_g)/R$ = 9.8 using the more accurate data from Kabo et al.[6] Lubchenko and Wolynes proposed to count beads from the entropy of fusion instead of at the glass transition.[14] Assuming an entropy of melting per particle for Lennard-Jones spheres, they obtained $S_{LJ} = 1.68k_B$, and hence, $N_{beads} = \Delta S_m/(1.68R)$. Because ΔS_m = 69.23 J/(K·mol) for [bmim][PF_6],[6] one obtained N_{beads} = 4.96. Therefore, the number of beads calculated from the entropy of fusion was one-half of that directly estimated from the glass-transition discontinuity $\Delta C_p(T_g)/R$. Very interestingly, this is exactly what we recently found in a family of alkyl-cyclohexanes.[11]

Another interesting physical magnitude of a glass-forming liquid is its fragility index m[15] (essentially, the activation energy at the glass transition in units of k_BT_g). The fragility of [bmim]$^+$-based room temperature ionic liquids has been estimated by using the viscosity measurements by Angell et al.[16] When these data, the recent data from Harris et al.,[17] and unpublished data from Gordon et al.[18] were combined, we modeled the viscosity dependence in terms of the Vogel−Fulcher−Tamman law: $\ln \eta = \ln \eta_o + DT_o/(T - T_o)$, where D is the Angell strength parameter that is large for *strong* materials and small for *fragile* ones.[16,19] The obtained parameters are D = 6.13 and T_o = 165.1 K. Harris et al. reported D = 7.0 and T_o = 161.8 K.[17] These values for D are consistent with a moderately fragile system.

We can estimate the fragility of [bmim][PF_6] from the thermodynamic data by using some successfully tested phenomenological relations. First, from a survey of 44 different glass-forming liquids, Wang and Angell[20] found an empirical relation between the fragility and thermodynamic data at the glass transition and the melting point

$$m = 56\frac{T_g}{\Delta H_m}\Delta C_p \qquad (3)$$

where ΔH_m is the enthalpy of melting. On the other hand, Wolynes and co-workers[14,21] also successfully predicted and tested a similar correlation between the supercooled liquid-fragility index m and the basic thermodynamic magnitudes:

$$m = 34.7\frac{T_m}{\Delta H_m}\Delta C_p \equiv 34.7\frac{\Delta C_p}{\Delta S_m} \qquad (4)$$

If we put the above-mentioned thermodynamic data from [bmim][PF_6] in these two scaling relations (eqs 3 and 4), a fragility index m of 44 or 41 is obtained, respectively. This value, which is similar to that found in *n*-propanol[21] or in alkyl-cyclohexanes,[11] was characteristic of a moderately strong liquid rather than a fragile liquid. Studying longer side chain imidazolium based salts, Moura Ramos et al.[22] found fragility indexes of the order of 50, which is consistent with our thermodynamic findings.

Upon successful formation of the amorphous glass, the short range order in [bmim][PF_6] was investigated using both neutron and X-ray diffraction. WANS data for the amorphous glass and the liquid of fully deuterated [bmim][PF_6] at selected temperatures are plotted in Figure 2. The WANS data are characterized by the occurrence of two amorphous halos that are related to structural correlations. At 50 K, a strong peak is centered at $Q \sim$ 1.5 Å^{-1}, which corresponds to a spatial correlation of $r = 2\pi/Q$ = 4.1 Å. At smaller Q values, another peak is found at the same temperature at $Q \sim$ 1.0 Å^{-1}, which corresponds to a spatial correlation of $r = 2\pi/Q$ = 6.4 Å. These spatial correlations are considered to be the fingerprint of residual order at a microscopic level in the morphology of liquid [bmim][PF_6].

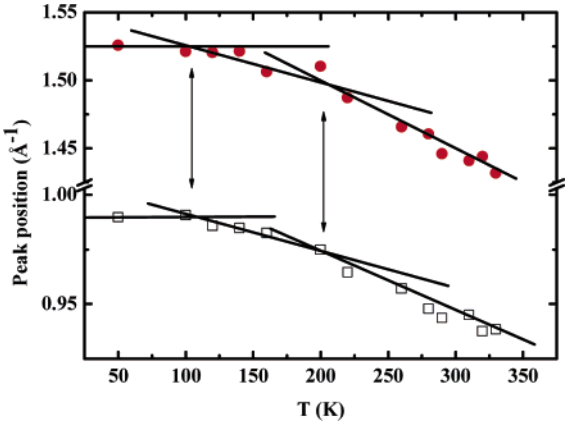

Figure 3. Temperature dependence of the positions of the two WANS peaks. The lines provide a phenomenological description of the data in terms of linear temperature dependences that highlight the existence of three different ranges in the morphology dependence from temperature.

This is common for a wide range of ionic liquids and molten salts, whereby, in their liquid state, at least part of the spatial order that characterizes the crystalline phase is preserved.[23] For example, Kochi et al.[24] assigned the $Q \sim 1.5$ Å^{-1} peak, which was observed with X-ray diffraction,[25] to the plane-to-plane distance between imidazolium rings that are supposed to be quasi stacked even in the liquid state. The same interpretation was derived from the analysis of the structural data in [emim][NO_3] in which the interplane distance between imidazolium rings was found to be ca. 4.5 Å.[26] On the other hand, many simulation studies focus on indicating this characteristic distance as related to the first solvation shell of the $[PF_6]^-$ anion around the imidazolium ring,[27,28] while the cation−cation correlation shows a characteristic distance of ca. 6.3 Å.[28] This is not strongly dependent on the length of the alkyl side chain as similar cation−cation correlations are observed for dimethyl imidazolium hexafluorophosphate.[29] It is clear that more experimental data are required to discriminate between these models.

Both diffraction peaks show a distinct temperature dependence. It is clear that only above the glass transition temperature major structural changes occur and this leads to a shift of the peaks. The two amorphous halos may be described with two Gaussian functions, and their positions are reported in Figure 3 as a function of the temperature. The two peaks show a similar behavior, and three temperature regimes exist, that is, between 0 and ca. 100 K where negligible temperature dependence can be observed, between 100 and 200 K where a distinct *T*-dependence is observed, and above 200 K where a second *T*-dependence is found. Interestingly, these observations resemble the characterization (by means of QENS) of similar temperature intervals between 0 and 400 K that are associated with the activation of localized and diffusive dynamic processes (vide infra). Such a close connection between morphological and dynamic features in the behavior of [bmim][PF_6] already has been highlighted in our previous study on longer alkyl chain imidazolium derivatives[30] and more recently has been proposed on the basis of molecular dynamics simulations of [bmim][PF_6][31] in which a hierarchy of processes has been found to characterize the dynamics. Furthermore, above ca. 200 K, a strong increase of the low Q plateau level (obtained as the average of $S(Q)$ between 0.6 and 0.7 Å^{-1}) can be observed (see inset of Figure 2). Such a feature can be related either to a strong temperature dependence of the sample compressibility or to the progressive development of an intermediate range order (IRO), that is, some

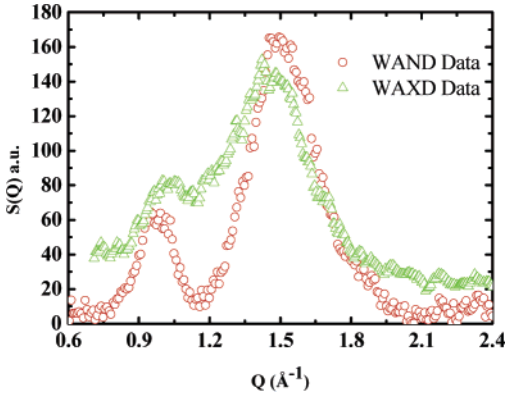

Figure 4. Comparison between WANS and WAXS data from liquid [bmim][PF_6] at 200 K.

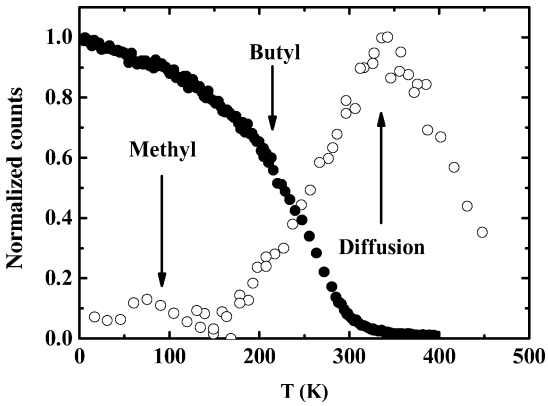

Figure 5. EFES (filled symbols) and IFES (empty symbols) collected from glassy [bmim][PF_6] at $Q = 1.23$ Å^{-1} and energy resolution of ca. 1 μeV. Above the glass transition, three temperature ranges can be distinguished that correspond to the activation of two low-temperature local relaxations (methyl and butyl groups) and of the diffusive relaxation.

structural correlations that progressively develop as the temperature increases above the glass transition. Though there is no experimental evidence to support the existence of IRO in RTILs, molecular dynamics simulations[28] highlighted the presence of a prepeak in the low Q region ($Q \sim 0.7$ Å^{-1}) in [bmim]Cl. Such an observation was rationalized in terms of a microphase separation because of the segregation of the sufficiently long alkyl chains. Further diffraction studies that focus on this relevant Q range will be necessary to better investigate this point.

X-ray diffraction data also were collected for the glassy and liquid sample over a smaller temperature range (from 180 to 210 K), and these data reflect the same features that were described for WANS data. They qualitatively resemble recently reported X-ray data for the same sample at 294 K.[25] In Figure 4, a comparison between WANS and wide angle X-ray scattering (WAXS) data from liquid [bmim][PF_6] at 200 K is reported.

The relaxation dynamics of glassy [bmim][PF_6] has been probed using QENS.[12] In Figure 5 elastic fixed energy (EFE) data and inelastic fixed energy (IFE) data with the same instrumental resolution are plotted for $Q = 1.29$ Å^{-1}. The occurrence of a relaxation process in the two kinds of experiments is associated with different features. In the case of the EFES, a relaxation process induces a steplike decrease of the signal. In contrast, in the case of the IFES, the same relaxation process would be associated with the presence of a peak. Both data sets indicate the occurrence of relaxation processes already at temperatures as low as 50 K.

Taking advantage of selective deuteriation either on the side methyl or on the side butyl group, we recently showed that the low-temperature features ($T < 100$ K) are related to the side methyl group relaxation.[12] The same techniques were used to characterize a higher temperature process that was associated with the butyl group relaxation and the diffusive relaxation occurring above the glass transition. These results were in good agreement with recent dielectric spectroscopy (DS) data collected over a wide frequency/temperature range on the same material.[32] In the case of [bmim][PF_6], this study highlighted the existence of two dielectric processes. Above the glass transition, the ionic conductivity followed a distinct non-Arrhenius trend that corresponded to the VTF behavior observed by QENS for the diffusive relaxation, whereas below T_g, an Arrhenius process was characterized by D. S. Rivera et al.,[32] who tentatively relate this finding to the butyl side chain relaxation, in agreement with our interpretation of the QENS data. A recent ab initio investigation[33] of [bmim][PF_6] highlighted the comparable stability of the trans and gauche conformations of the butyl chain in the liquid state. The complex motion associated with the transitions between comparably stable chain conformations might be responsible for the observed relaxation.

This interpretation of the QENS data also might be the key to rationalize the dynamics−structure interplay that was previously mentioned. We tentatively associate the three temperature regimes derived from the analysis of Figure 3 to the complex dynamic behavior that was observed through QENS. In the low-temperature range (regime I, 0−100 K) in which no appreciable structural changes occur, no dynamics processes occur apart from the activation of the highly localized methyl group rotation. Such a glassy state maintains a rigid structural configuration without major changes in the diffraction pattern. Conversely, in the temperature regime between ca. 100 K and the glass transition (regime II, 100−200 K), the methyl group rotation occurs and the butyl side chain overcomes its activation energy and relaxes with a complex motion, exploring different conformations (e.g., Figure 7 of ref 28). These localized relaxation processes are active well below the glass transition, thus implying that despite the freezing of the diffusive motions, substantial local mobility remains. Such an effect seems to affect the microscopic structural features of [bmim][PF_6], observed in Figure 3. Finally, above the glass transition (regime III, >200 K), diffusive motions become activated and correspondingly determine a change in the temperature dependence of the structure.

In the present study, we provide new information on the strong coupling between dynamical properties of [bmim][PF_6] and its microscopic morphology. Many techniques are converging in highlighting the existence of a hierarchy of relaxation processes in [bmim][PF_6]. Our QENS study[12] revealed three processes (methyl, butyl, and diffusion). ^{13}C NMR,[34] molecular dynamics,[27,28,31] and DS[32] identified the existence of two dynamic processes: long time diffusive dynamics and a much faster localized process associated with conformational transitions in the butyl chain.

II. Crystal Phases. Evidences of crystal polymorphism in [bmim]X salts (in particular, for X = Cl and Br) have been obtained in the past.[35−37] In the case of [bmim][PF_6], a recent report indicated that upon heating the amorphous glass, a crystalline phase is obtained at ca. 233 K.[38] The same authors observed a further phase transition at ca. 263 K but provided no further information on this phase.[38] Another report[24] described a crystalline phase of [bmim][PF_6] that corresponds to the one previously observed by Winterton et al.[38] These authors obtained their crystalline phase by shock-induced crystallization of a glassy sample at 243 K. In the present report, we successfully isolated two crystalline phases in [bmim][PF_6] and investigated them with calorimetric and diffraction methods.

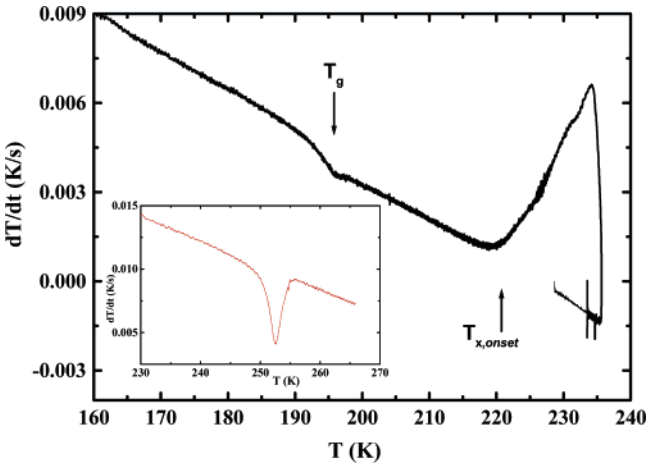

Figure 6. Continuous calorimetric measurement that highlights the crystallization process of [bmim][PF_6] upon heating from the glassy state. The glass transition can be observed at $T_g = 194$ K and followed by crystallization (cr-II) that starts at $T_{x,onset} = 220$ K. The inset shows the endothermic process at around 252 K observed when heating the crystalline phase cr-II, which is assigned to the cr-II to cr-I transition.

After the liquid sample was cooled down to 260 K and after the temperature was kept constant at that value for a few hours, [bmim][PF_6] crystallized with a crystallization enthalpy of 42 J g^{-1}. We indicated this crystalline phase as cr-I. It will be shown that this crystalline phase was different from the one probed with X-ray diffraction by both the Winterton[38] and the Kochi[24] groups. We also observed that upon heating the amorphous glass, a crystalline phase formed at ca. 220 K, which we identified as cr-II. Diffraction techniques were used to determine that this crystalline phase corresponded to the one that was characterized by refs 38 and 24. The previous thermodynamic characterization[6] of [bmim][PF_6] did not highlight the difference between these two crystalline phases but investigated the crystalline phase obtained through heating of the glassy amorphous state (cr-II). The calorimetric study by Winterton et al.[38] led to the observation that upon further heating of cr-II, a phase transition at ca. 263 K was observed. We can now state that they observed the transition into the crystalline phase cr-I.

In Figure 6, one example of our quasi-adiabatic, continuous calorimetry measurements on the crystallization process of the amorphous glass is reported: upon heating the amorphous glass from 160 K, one can observe (i) the glass−liquid transition at 194 K and, in agreement with previous studies, (ii) the crystallization event (cr-II formation) with an onset temperature of 220 K and a crystallization enthalpy of ca. 34 J g^{-1}. Indications of a crystal to crystal transition (cr-II to cr-I, i.e., from the low-temperature stable phase to the high-temperature one) upon further heating can be observed at 252 K with an enthalpy of ca. −5 J g^{-1} (shown in the inset of Figure 6).

We have further indication that cr-I and cr-II are different crystalline phases. In particular, we observed that cr-I exhibits exothermic/endothermic transitions when cooling/heating (black and red lines in Figure 7) at 177 and 217.5 K with corresponding enthalpies of ca. 1.7 and 1.0 J g^{-1}, respectively. The nature of these transitions, which were not previously identified for any RTIL, is not clear yet, and further investigation is in progress

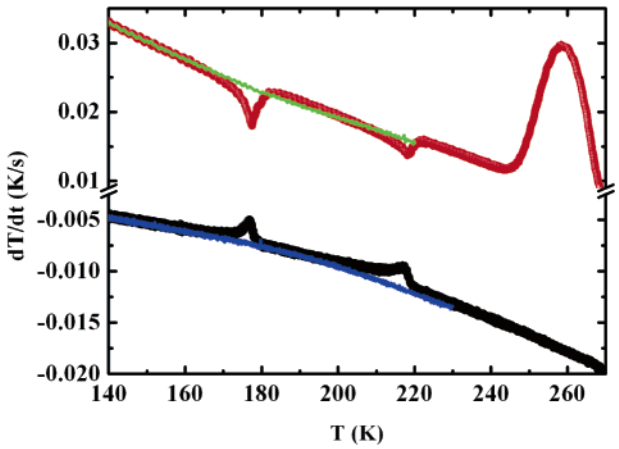

Figure 7. Comparison of the quasi-adiabatic, continuous calorimetry measurements from the two crystalline phases obtained for [bmim][PF_6] upon cooling and heating. It can be observed that upon the cooling/heating of phase cr-I, two exothermic/endothermic transitions occur (black and red lines, respectively). In comparison, the same temperature path does not induce any transition for the cr-II phase (blue and green lines).

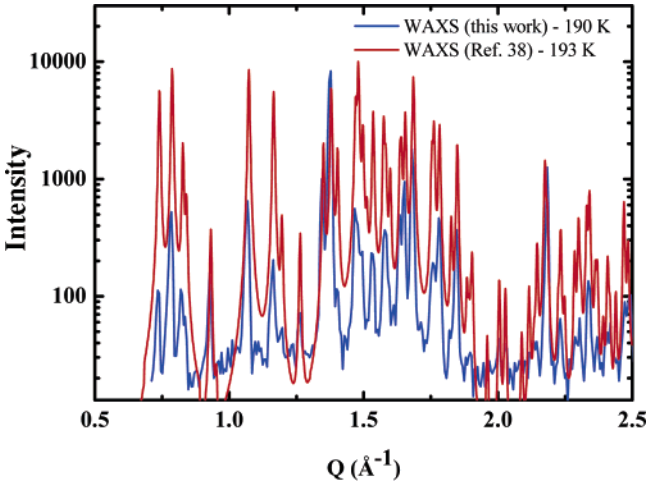

Figure 8. WAXS powder diffraction data for phase cr-I of [bmim][PF_6] at 190 K. The data are compared to the powder-averaged data obtained by Winterton et al.[38] at 180 K, which indicates that the two sets of measurements refer to the same crystalline phase.

to understand these observations, which, nevertheless, were fully reproducible. On the other hand, the phase cr-II does not show any feature at these temperatures (blue and green lines in Figure 7). Upon heating of the quenched cr-I, a strong exothermic event occurs at $T = 246$ K with an enthalpy of 27 J g^{-1}. Such a process can be related to a cr-I → cr-II transition.

Once the cr-II form is prepared and quenched, upon heating (with no evidence of endothermic transitions at 177 and 217.5 K), this sample exhibits an endothermic transition at 252 K (enthalpy = −5 J g^{-1}) that is presumably related to the cr-II → cr-I transition. Once quenched, the newly formed samples exhibit the typical transitions at 177 and 217.5 K, which can be considered fingerprints of phase cr-I. Such a complexity in the phase diagram of [bmim][PF_6] has been confirmed by X-ray powder diffraction. Single-crystal X-ray diffraction on [bmim]Cl and [bmim]Br highlighted the existence of two different crystal phases for these salts.[35−37] Single-crystal X-ray diffraction of a crystalline phase of [bmim][PF_6] also has been reported recently.[38,24]

We obtained qualitative indication of a crystal polymorphism in [bmim][PF_6] in a previous report dealing with QENS characterization of relaxation processes in this ionic liquid.[39] Upon heating the glass, we observed two crystallization steps that corresponded to the experimental findings reported by Winterton[38] and to the present report. By applying the experimental protocols identified by the previously described quasi-adiabatic calorimetry measurements, we also succeeded in obtaining the powder diffraction patterns from the two crystalline phases. These systems also were studied as a function of temperature.

Upon aging of liquid [bmim][PF_6] at 260 K for few hours, we succeeded in preparing cr-I. In Figure 8, powder diffraction data for this phase are reported for $T = 190$ K. Conversion of single-crystal data from ref 38 into a powder spectrum collected at 180 K agree well with our data set at 190 K. This crystalline phase has been identified as triclinic with structural parameters: $a = 8.774$ Å, $b = 8.944$ Å, $c = 9.032$ Å and $\alpha = 95.95°$, $\beta = 114.93°$, $\gamma = 103.01°$ at 180 K.[38] We note that longer chain 1-methyl-3-alkyl imidazolium hexafluorophosphate ([C_{12}mim][PF_6][40] and [C_{14}mim][PF_6][30]) show a monoclinic crystalline structure. The crystal structure of the latter samples consists of imidazolium ring layers that are separated by interdigitating alkyl chains. The interlayer separation corresponds to the *a* unit cell parameter. This parameter is found[40] to depend linearly on the alkyl chain length, *n*. We observe that by linearly extrapolating such a dependence down to $n = 4$ (for the butyl chain), a value of interlayer distance of ca. 15 Å would be expected. Such a phenomenological observation indicates that the crystalline organization of hexafluorophosphate-based 1-alkyl-3-methyl imidazolium salts strongly depends on the alkyl chain length and that this is different for short and long alkyl chain samples. This finding might be rationalized when considering that in long alkyl chain salts a high degree of alkyl chain/chain interaction affects the structure, which leads to liquid crystalline behavior,[40,41] while in short chain salts, the ordering is mainly driven by electrostatic interactions. The intermediate alkyl chain length in $[bmim]^+$ leads to a hybrid degree of ordering that resembles both the short and the long alkyl chain behavior.[24]

In agreement with the calorimetric findings presented herein, upon heating the crystalline sample (cr-I) from 160 to 240 K, no structural change occurred (as indicated by both WAXS and WANS), and only one crystalline phase (cr-I) was stable in this temperature range. The cr-II phase that develops upon heating the amorphous glassy material also has been characterized with powder X-ray diffraction. The corresponding sample was prepared by quenching the liquid at 180 K, and X-ray data were collected at different temperatures upon heating. In the range 180−215 K, the sample remained amorphous, but at 220 K, crystallization occurred (leading to cr-II) with a morphology that is different from the morphology of the phase cr-I, which is shown in Figure 9 for $T = 230$ K.

We showed that our powder X-ray diffraction data for phase cr-I agree with the crystalline order found in refs 38 and 24. We are now in the process of solving the structure of phase cr-II on the basis of the present powder diffraction data, and this will be the subject of a following report. In agreement with the calorimetric findings, when the temperature of the sample in the phase cr-II is increased, a phase transition corresponding to the transition cr-II → cr-I at ca. 245 K occurs. In Figure 10, a portion of the diffraction data corresponding to the heating of cr-II across the cr-II → cr-I transition is presented. It is shown that upon heating across $T = 250$ K, the peak at 0.80 $Å^{-1}$ (a fingerprint for phase cr-II) disappears, while the peaks at 0.73, 0.78, and 0.82 $Å^{-1}$ (fingerprints for phase cr-I) progressively develop. This temperature corresponds to the one where the

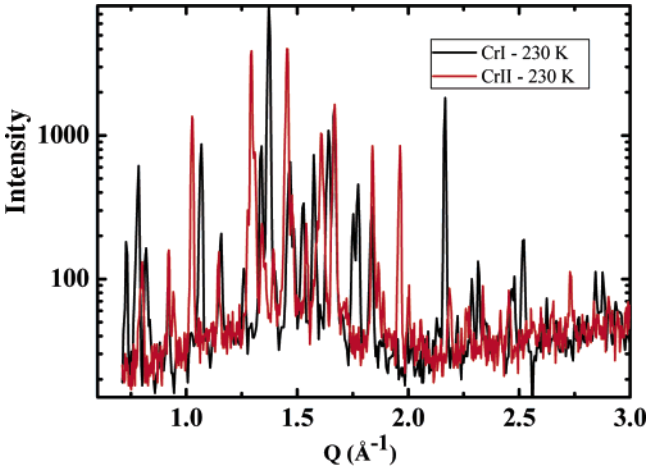

Figure 9. Comparison between X-ray powder diffraction data from the two polymorphs of [bmim][PF_6] (cr-I and cr-II) at 230 K.

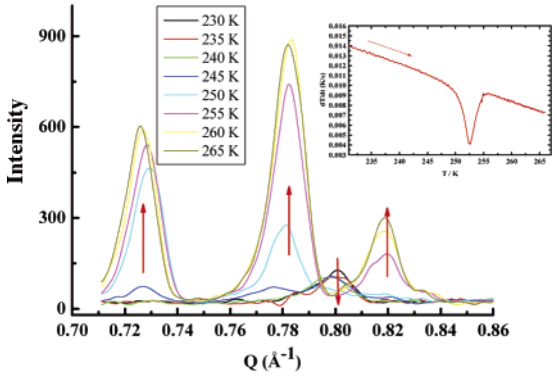

Figure 10. Temperature dependence of a portion of the WAXS data that corresponds to the heating of crystalline [bmim][PF_6] in its phase cr-II across the cr-II → cr-I transition at $T = 250$ K. In the inset, the calorimetry data indicating the transition from cr-II to cr-I are reported.

calorimetry measurements indicate the transition from cr-II to cr-I (see the inset of Figure 6).

Previously, the importance of crystal polymorphism in rationalizing their good glass-forming ability and their highly hindered crystallization has been highlighted.[35−37] This polymorphism has been related to a different local conformation of the side butyl chain in a series of $[bmim]^+$-based RTILs. In the case of [bmim]Cl, one polymorph shows an anti configuration for all the C−C bonds in the alkyl chain. The other polymorph differs from the first for the alkyl chain conformation around the $C_\alpha-C_\beta$ bond.[35]

Very recently, a pertinent paper from Saito et al.[42] reported on low-temperature heat specific measurements on 1-hexyl-3-methyl imidazolium bis(trifluoromethylsulfonyl)imide ([hmim][Tf_2N]). The authors also characterized the existence of crystal polymorphism in their high-purity sample, because they found indications of melting of two different crystalline phases, although they propose that one of them is a metastable phase.

Conclusions

An optimal exploitation of the solvent performances of room-temperature ionic liquids will require a detailed knowledge of their phase diagram and of the range of stability of the different amorphous glassy, crystalline, and liquid phases. In this report, we extend the present knowledge on the complex nature of the phase diagram of [bmim][PF_6], which is a well-known representative of the class of RTIL.

Thermodynamic, structural, and dynamical information is obtained for this salt in its amorphous glassy and liquid state, taking advantage of quasi-adiabatic, continuous calorimetry, and X-ray and neutron scattering. We provide information on the thermodynamic properties of the glass−liquid transition, complementing the recently derived data from ref 6.

We extended the structural study on the structure of glassy and liquid [bmim][PF_6] from that reported by Billard et al.[25] with complementary neutron and X-ray diffraction measurements over a wide temperature range that accessed the temperature dependence of the medium range structural correlations in this structured material. Our results confirmed the view that RTILs in general, and [bmim][PF_6] in particular, show a substantial degree of order even in their amorphous states, which resembles the crystalline order. These results were in agreement with recent experimental and simulation work on this and similar RTILs. A strong correlation between order and localized relaxation processes of the imidazolium salt also has been found: the characteristic distances accessed by both X-ray and neutron scattering showed a temperature dependence that strongly reflected the activation of highly-localized processes such as the butyl group relaxation and the diffusive dynamics, as determined by QENS.

A complex crystal polymorphism also has been characterized for [bmim][PF_6]. The formation of two different stable crystalline phases has been characterized by means of both calorimetry and X-ray diffraction techniques. Upon isothermal treatment of the supercooled liquid, a stable crystalline phase formed (cr-I). This phase showed an X-ray pattern that corresponds to the single-crystal pattern, which has been investigated in refs 38 and 24. The temperature evolution of this phase has been studied, and it shows a strong exothermic transition at 246 K to another crystalline phase (cr-II) that was detected previously[38] but was not investigated further. The phase cr-I reproducibly shows exothermic/endothermic peaks when cooling/heating at 177 and 217.5 K with corresponding enthalpies of ca. 1.7 and 1.0 J g^{-1}, respectively.

The crystalline phase cr-II was also prepared in a stable way by heating the supercooled liquid: at 220 K the liquid will show a transition to a crystalline phase with an X-ray pattern that is different from the one of cr-I. This phase does not show the two characteristic transitions at 177 and 217.5 K. Upon heating this crystalline phase, the transition to cr-I can be observed via both calorimetry and X-ray diffraction.

These results provide a strong experimental basis to the exploration of the wealth of features of the phase diagram of RTILs and to the further study of longer alkyl chain salts.

Acknowledgment. A.T., A.M., V.R.-M., and M.A.R. were financially supported by the Spanish Ministery of Education and Science within Project BFM2003-04622. This work is partially based on experiments performed at the Swiss spallation neutron source SINQ, Paul Scherrer Institute, Villigen, Switzerland. The ILL is acknowledged for providing financial support and beam time at IN10 and IN16. The skillful support from the local contact, Dr. M. A. Gonzalez, is acknowledged. We also acknowledge the support of the European Community, Access to Research Infrastructure Action of the Improving Human Potential Programme (Grant HPRI-2001-00175), which funded the access to the FZJ facilities and the helpful support of the local contact of the BSS spectrometer, Dr. H. Grimm. C.H. and M.N. acknowledge funding via an EPSRC portfolio grant.

References and Notes

(1) *Ionic Liquids in Synthesis*; Wasserscheid, P.; Welton, T., Eds.; Wiley-VCH: Weinheim, Germany, 2003.

(2) Welton, T. *Chem. Rev.* **1999**, *99*, 2071.
(3) Suarez, P. A. A.; Dullius, J. E. L.; Einloft, S.; De Souza, R. F.; Dupont, J. *Polyhedron* **1996**, *15*, 1217.
(4) Huddleston, J. G.; Visser, A. E.; Reichert, W. M.; Willauer, H. D.; Broker, G. A.; Rogers, R. D. *Green Chem.*, **2001**, *3*, 156.
(5) Paulechka, Y. U.; Kabo, G. J.; Blokhin, A. V.; Vydrov, O. A.; Magee, J. W.; Frenkel, M. *J. Chem. Eng. Data* **2003**, *48*, 457.
(6) Kabo, G. J.; Blokhin, A. V.; Paulechka, Y. U.; Kabo, A. G.; Shymanovich, M. P.; Magee, J. W. *J. Chem. Eng. Data* **2004**, *49*, 453.
(7) (a) Villagràn, C.; Deetlefs, M.; Pitner, W.; Hardacre, C. *Anal. Chem.* **2004**, *76*, 2118. (b) Villagràn, C.; Banks, C. E.; Deetlefs, M.; Driver, G.; Compton, R. G.; Hardacre, C. submitted to ACS Symposium series Ionic Liquids: Progress and Prospects.
(8) Hardacre, C.; Holbrey, J. D.; McMath, S. E. J. *J. Chem. Soc., Chem. Commun.* **2001**, 367.
(9) Gordon, C. M.; Holbrey, J. D.; Kennedy, A. R.; Seddon, K. R. *J. Mater. Chem.* **1998**, *8*, 2627.
(10) Gmelin, E. *Thermochim. Acta* **1979**, *29*, 1.
(11) Mandanici, A.; Cutroni, M.; Triolo, A.; Rodriguez-Mora, V.; Ramos, M. A. *J. Chem. Phys.* **2006**, *125*, 054514.
(12) Triolo, A.; Russina, O.; Hardacre, C.; Nieuwenhuyzen, M.; Gonzalez, M. A.; Grimm, H. *J. Phys. Chem. B* **2005**, *109*, 22061.
(13) Fischer, P.; Keller, L.; Schefer, J.; Kohlòbrecher, J. *Neutron News* **2000**, *11*, 19; see also http://sinq.web.psi.ch/sinq/instr/dmc/dmc.html.
(14) Lubchenko, V.; and Wolynes, P. G. *J. Chem. Phys.* **2003**, *119*, 9088.
(15) Angell, C. A. *J. Non-Cryst. Solids* **1988**, *102*, 205.
(16) Xu, W.; Cooper, E. I.; Angell, C. A. *J. Phys. Chem. B* **2003**, *107*, 6170.
(17) Harris, K. R.; Woolf, L. A.; Kanakubo, M. *J. Chem. Eng. Data* **2005**, *50*, 1777.
(18) Gordon, C. M. Unpublished data, 2005.
(19) Angell, C. A. *Science* **1995**, *267*, 1924.
(20) Wang, L. M.; Angell, C. A. *J. Chem. Phys.* **2003**, *118*, 10353.
(21) Stevenson, J. D.; Wolynes, P. G. *J. Phys. Chem. B* **2005**, *109*, 15093.
(22) Moura Ramos, J. J.; Afonso, C. A. M.; Branco, L. C. *J. Therm. Anal.* **2003**, *71*, 659.
(23) (a) Biggin, S.; Enderby, J. E. *J. Phys. C: Solid State Phys.* **1982**, *15*, L305. (b) Rovere, M.; Tosi, M. P. *Rep. Prog. Phys.* **1986**, *49*, 1001. (c) Martin, J. D. In *Ionic Liquids: Industrial Applications of Green Solvents*; Rogers, R. D., Seddon, K. R., Eds.; American Chemical Society: San Diego, CA, 2002; pp 413−427. (d) Hefeng, L.; Kunquan, L.; Zhonghua, W.; Jun, D. *J. Phys. C: Solid State Phys.* **1994**, *6*, 3629. (e) Hardacre, C.; Holbrey, J. D.; McMath, S. E. J.; Bowron, D. T.; Soper, A. K. *J. Chem. Phys.* **2003**, *118*, 273.
(24) Dibrov, S. M.; Kochi, J. K. *Acta Crystallogr., Sect. C* **2006**, *62*, o19.
(25) Billard, I.; Moutiers, G.; Labet, A.; El Azzi, A.; Gaillard, C.; Mariet, C.; Lutzenkirchen, K. *Inorg. Chem.* **2003**, *42*, 1726.
(26) Wilkes, J. S.; Zaworotko, M. J. *J. Chem. Soc., Chem. Comm.* **1992**, 965.
(27) (a) Morrow, T. I.; Maginn, E. J. *J. Phys. Chem. B* **2002**, *106*, 12807. (b) Morrow, T. I.; Maginn, E. J. *J. Phys. Chem. B* **2003**, *107*, 9160.
(28) Urahata, S. M.; Ribeiro, M. C. C. *J. Chem. Phys.* **2004**, *120*, 1855.
(29) Hardacre, C.; McMath, S. E. J.; Nieuwenhuyzen, M.; Bowron, D. T.; Soper, A. K. *J. Phys. C* **2003**, *15*, S159.
(30) De Roche, J.; Gordon, C. M.; Imrie, C. T.; Ingram, M. D.; Kennedy, A. R.; Lo Celso, F.; Triolo, A. *Chem. Mater.* **2003**, *15*, 3089.
(31) Urahata, S. M.; Ribeiro, M. C. C. *J. Chem. Phys.* **2005**, *122*, 24511.
(32) Rivera, A.; Rossler, E. A. *Phys. Rev. B* **2006**, *73*, 212201.
(33) Berg, R. W.; Deetlefs, M.; Seddon, K. R.; Shim, I.; Thompson, J. M. *J. Phys. Chem. B* **2005**, *109*, 19018.
(34) Antony, J. H.; Mertens, D.; Dolle, A.; Wasserscheid, P.; Carper, W. R. *ChemPhysChem.* **2003**, *4*, 588.
(35) Holbrey, J. D.; Reichert, W. M.; Nieuwenhuyzen, M.; Johnston, S.; Seddon, K. R.; Rogers, R. D. *Chem. Commun.* **2003**, 1636.
(36) Saha, S.; Hayashi, S.; Kobayashi, A.; Hamaguchi, H. *Chem. Lett.* **2003**, *32*, 740.
(37) Hayashi, S.; Ozawa, R.; Hamaguchi, H. *Chem. Lett.* **2003**, *32*, 498.
(38) Choudhury, A. R.; Winterton, N.; Steiner, A.; Cooper, A. I.; Johnson K. A. *J. Am. Chem. Soc.* **2005**, *127*, 16792.
(39) Triolo, A.; Russina, O.; Arrighi, V.; Juranyi, F.; Janssen, S.; Gordon, C. M. *J. Chem. Phys.* **2003**, *119*, 8549.
(40) Gordon, C. M.; Holbrey, J. D.; Kennedy, A. R.; Seddon, K. R. *J. Mater. Chem.* **1998**, *8*, 2627.
(41) Bradley, A. E.; Hardacre, C.; Holbrey, J. D.; Johnston, S.; McMath, S. E. J.; Nieuwenhuyzen, M. *Chem. Mater.* **2002**, *14*, 629.
(42) Shimizu, Y.; Ohte, Y.; Yamamura, Y.; Saito, K.; Atake, T. *J. Phys. Chem. B* **2006**, *110*, 13970.